# Lower Turbulent Zones Associated with Mountain Lee Waves[1]

Peter F. Lester and William A. Fingerhut, San Jose State University, San Jose, California

Presented at the 14th OSTIV Congress, Waikerie, Australia (1974)

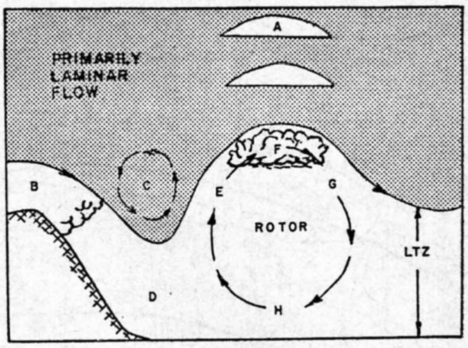

Figure 1. Idealized cross section of the LTZ. A. Lenticular Clouds, B. Cap cloud, C. reversed rotor, D. Region of gusty surface winds, E. Region of strong updraft and extreme turbulence, F. Rotor or roll cloud, G. Region of strong downdraft and severe turbulence, H. Lower portion of rotor circulation and occasionally reversed surface winds.

## Introduction

Mountain lee waves are frequently accompanied by a lower turbulent zone (LTZ). The LTZ ist a highly turbulent region of nearly neutral stability found immediately to the lee of the mountains between the ground and an elevated stable layer in which the wave motion is occurring (Kuettner, 1959).

Figure 1 summarizes the general characteristics of the LTZ. It is based primarily on studies conducted prior to 1960, when instrumentation and data recording systems were not capable of resolving horizontal scales less than a few kilometres (see, e.g., Holmboe and Klieforth, 1957). As a result, much of the knowledge of the small scale structure of the LTZ is semiquantitative (see Alaka, 1960, for a detailed review). This problem is compounded by the intense turbulence found in the LTZ which has limited the number of planned penetrations of that phenomenon with instrumented aircraft.

During the past decade, aircraft observational systems have been greatly improved (see, e.g., Vinnechenko et al., 1973). The resolution of motions over scales of only a few metres is now possible. Also, during this period, intensive studies of lee waves and chinook winds have been undertaken in the Colorado Rocky Mountains (Kuettner and Lilly, 1968; Lilly et al., 1971; Lilly and Zipser, 1972) with penetrations of the LTZ by instrumented aircraft. The present paper presents a detailed analysis of one LTZ case and summarizes the principal characteristics of five other cases.

## Data and Analyses

Data were obtained by an instrumented Queen Air A80 flown under the auspices of the National Center for Atmospheric Research (NCAR)[2]. The aircraft instrumentation is described in detail by Burris et al. (1973). The following parameters were either measured directly or derived from measured parameters recorded at rate of 8 $\sec^{-1}$: aircraft altitude and position, potential temperature, horizontal wind velocity and longitudinal gust velocity.

A low pass filter was applied to the wind data to eliminate noise inherent in the Doppler navigation system and to isolate the mesoscale structure of the LTZ. Perturbations with wave lengths less than 4.7 km were eliminated in the filtering process. Potential temperature data were similarly smoothed. The filtering technique has been described in detail by Lester (1972). Cross sections of wind speed and direction and potential temperature along the aircraft tracks were constructed and analyzed objectively via computer.

In order to examine the turbulence structure of the LTZ, longitudinal gust velocities (u') were obtained by applying a high pass filter to the true air speed data to eliminate all fluctuations with wave lengths greater than about 850 m. The spatial distribution of the turbulence intensity was determined by computing the root-mean-square values of the longitudinal gust velocity (i.e., $\sqrt{\overline{u'^2}}$) over 3 km intervals and by analyzing these numbers in cross sectional form.

## The 8 December 1970 case

This case has been selected from a series of six LTZ cases examined in detail by Fingerhut and Lester (1973). It is unique in that the flight pattern of the investigating aircraft allowed the construction of multiple cross sections so that both temporal and spatial variations of the LTZ could be examined. Also, the case is intense (large amplitude lee waves, strong winds and turbulence) and the LTZ characteristics are well-defined. The flight plan for 8 Dec. 70 consisted of a series of four cross sections (three flight legs each) over the plains to the east of the Continental Divide between the altitudes of about 0.8 and 4.2 km above ground level (AGL). The flight tracks and the topography of the area are shown in Figure 2.

The synoptic conditions for 8 Dec 70 at 1700 MST are characterized by moderate westerly flow at 500 mb (Figure 3) and a nearly west-east cold front at the surface, immediately to the south of the study area (Figure 4). Although the slowly moving front was weak (note isotherms in Figure 4), significant changes in the structure of the LTZ occurred when it moved across the study area during the period of the aircraft flights (1148–1523 MST). From an inspection of previous surface charts (not shown), it appears that the earliest cross section (track 1 in Figure 2) was located ahead of the front while the other three cross sections were behind the front.

The potential temperature, wind and turbulence fields along flight tracks 1, 2 and 3 appear in Figures 5 through 7, respectively. The average terrain profile along each flight track is shown in each figure.

Figure 2. Topography and flight tracks (heavy solid lines) for 8 December 1970 investigation. Heights are in km (MSL). The Continental Divide is indicated by the dashed line. All subsequent cross sections are referenced to the longitude of JEFFCO (Jefferson County Airport).

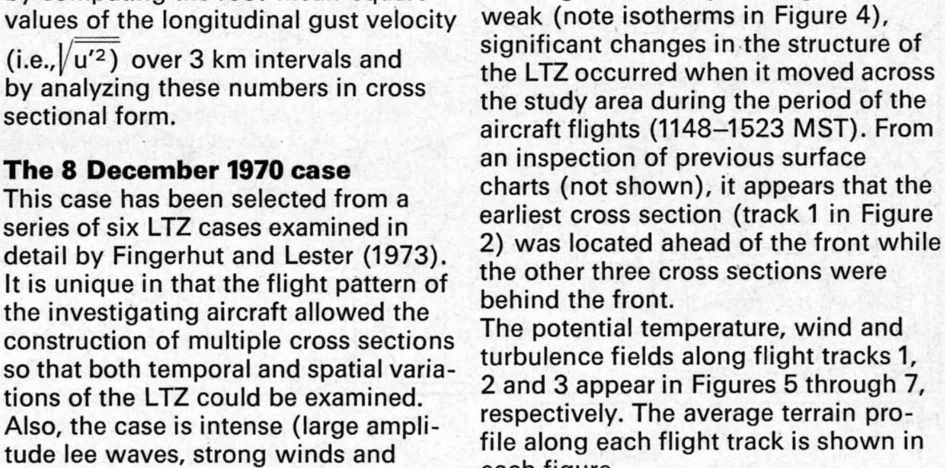

---

[1] This paper has also been published in the Journal of Applied Meteorology, USA.

[2] NCAR is operated by the University Corporation for Atmospheric Research under the sponsorship of the National Science Foundation.

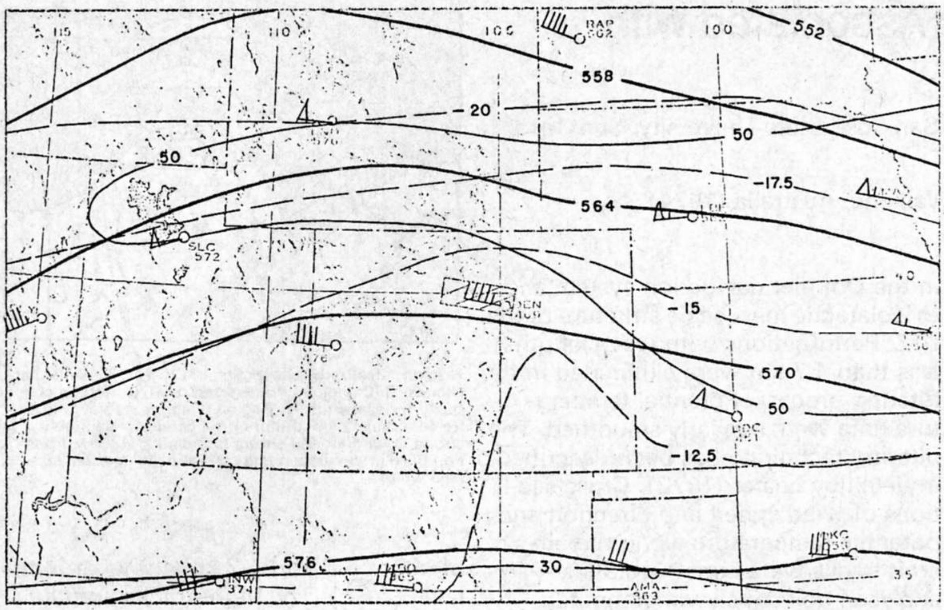

Figure 3

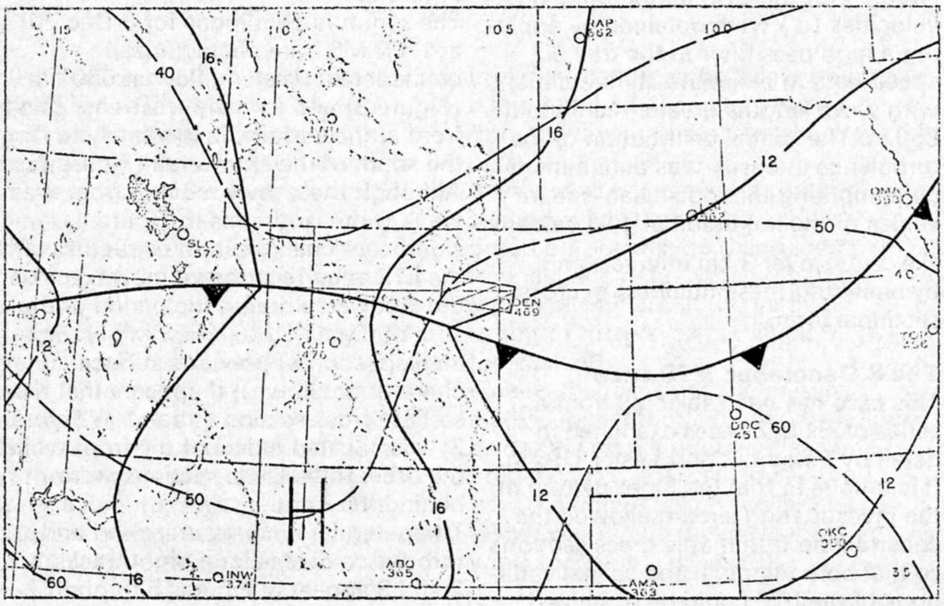

Figure 4

Figure 3. 500 mb analysis for 1700 MST, 8 December 1970. Heavy solid lines are geopotential height (decameters), thin solid lines are isotachs (knots) and dashed lines are isotherms (°C). The shaded box in the center of the Figure ist the study area.

Figure 4. Surface analysis for 1700 MST, 8 December 1970. Thin solid lines are sea level isobars (mb), and dashed lines are isotherms (F).

The isentropes may be interpreted as streamlines in the case of steady, inviscid, adiabatic flow. Although such is not the case within the turbulent LTZ near the earth's surface, the isentropes will be assumed to approximate the upper lee wave flow, at least during the period of data collection for each cross section.

A comparison of Figures 5, 6 and 7 reveals the effect of the frontal passage[3]. Recalling that cross sections 2 and 3 (Figures 6 and 7) represent conditions behind the front, one notes the increase of lee wave length (from about 20 km to 32 km), of double amplitude (from about 1 to 1.5 km), and of the overall turbulence intensity and wind speeds at upper levels. The wind direction (not shown in Figures 5 and 6), which was from the west at the two earlier times, shifted to the WNW in the lower levels at the time of cross section 3 (Figure 7).

Although cross section 2 is about 20 km north of cross sections 1 and 3 (see Figure 2) it was not possible to isolate spatial changes in the LTZ structure due to variations in upstream terrain. The large synoptic changes have apparently masked any effects due to topographic irregularities.

The LTZ structure and its temporal variations closely parallel that of the lee waves, that is, as the lee waves intensified, so did the LTZ. Taking the 306K isentrope as the 'top' of the LTZ in Figures 5–8, it is noted that the depth of the LTZ varies from a few hundred metres below the wave troughs to more than 2.5 km AGL in the crests. The LTZ extends at least 40 km downstream of the first lee wave trough.

Near neutral stability was found with n the LTZ with weakly unstable layers at lower levels. Holmboe and Klieforth (1957) have described the problem of implying streamlines from isentropes within the LTZ (i.e., the rotor), because of the low stability and intense mixing. However, the wind speed minima in Figures 5–7 strongly suggest the existence of a rotor circulation, particularly in the case of cross section 3 (Figure 7). Wind speed maxima tend to fall into the region of strongest potential temperature gradient at the top of the LTZ. Vertical wind shears and horizontal wind speed variations along the aircraft tracks are large, reaching values of $1.5 \cdot 10^{-2}$ sec$^{-1}$ and $4.0 \cdot 10^{-3}$ sec$^{-1}$, respectively. It should be noted that these values are representative of the mesoscale (smoothed) structure of the LTZ, and that actual magnitudes are even larger, due to smaller scale turbulent fluctuations.

The turbulent structure of the LTZ is revealed by the $\sqrt{u'^2}$ analyses in the upper cross section of each figure. Subjective pilot and observer reports of turbulence (symbols in $\sqrt{u'^2}$ diagrams) were found to be related to $\sqrt{u'^2}$ values as follows:

$0.4 < \sqrt{u'^2} < 0.9$ m/s (light)
$0.9 \le \sqrt{u'^2} < 1.5$ m/s (moderate)
$\sqrt{u'^2} \ge 1.5$ m/s (severe)

These classifications apply only to the present work since they depend on the characteristics of a given aircraft and the filter applied to the true air speed data.

In addition to the general increase in turbulence following the frontal pas-

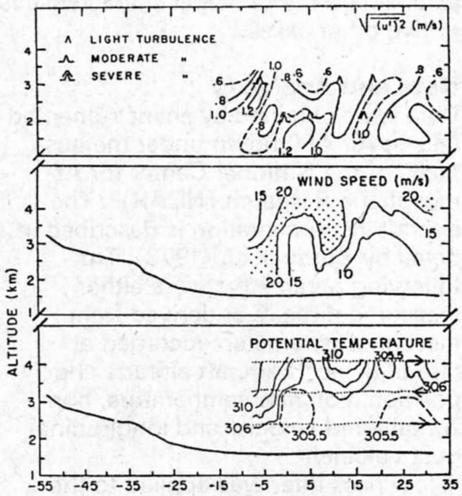

Figure 5. Cross section 1. Mesoscale flow pattern for 1148–1233 MST, 8 December 1970. Dotted lines indicate aircraft paths. Regions of maximum wind speed are shaded. The heavy solid line below the potential temperature analysis represents the topography profile along the aircraft track.

---

[3] In another case (20 Jan. 71), the passage of a much stronger and rapidly moving cold front, had an opposite effect, i.e., wave lengths, wave amplitudes, the depth of the LTZ and turbulence levels decreased markedly as the front passed.

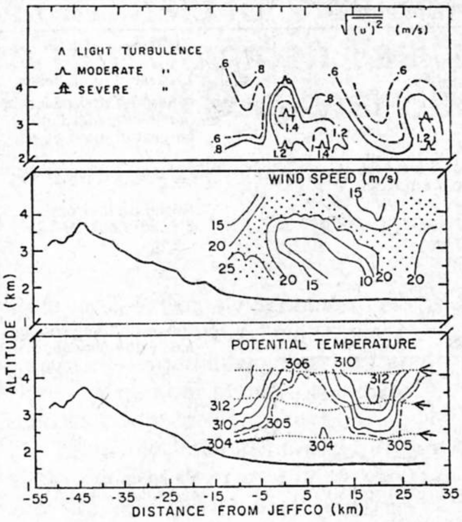

Figure 6. Cross section 2. Same as Figure 5, but for 1239–1448 MST.

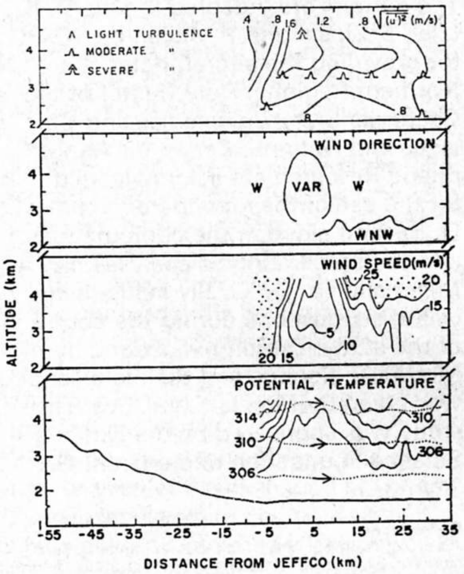

Figure 7. Cross section 3. Same as Figure 5, but for 1339–1523 MST.

sage, the height of the upper boundary of the turbulence region increased from about 2.5 km MSL (Figure 5) to more than 4 km MSL (Figure 7). The wind speed minimum was also displaced upward. Separate turbulence maxima appear to have been associated with the rotor and with the updraft region. This double maximum is particularly marked in cross sections 1 and 2 (Figures 5 and 6). Minimum turbulence values were observed in and near the troughs of the upper lee waves.

Large gradients in turbulence intensity were found near the undulating upper boundary of the LTZ and were particularly strong in the updraft region.

Because $\sqrt{u'^2}$ was computed over 3 km (about 30 second) intervals, the rapidity of the onset of the turbulence is underestimated, especially for aircraft flying downstream into the primary updraft. Figure 8 is presented as a more detailed illustration of this effect. One second averages of true air speed (TAS) and potential temperature ($\theta$) are shown for the upper flight leg of cross section 3 (Figure 7).

Cross section 4 (Figure 9), oriented approximately parallel to the ridgeline, is located in the lee wave trough at the upstream end of the previous cross sections (see Figure 2). It is suspected that the wave trough is the first to the lee of the mountains, but this could not be verified from the available data. Note the relatively strong potential temperature gradient, strong winds and intense turbulence at the lowest levels. The LTZ was evidently only a few hundred metres deep in the trough and the strongest winds were confined to the lowest levels with large negative vertical wind shears above. The slight slope of the isentropes may be due either to the slope of the cold front or to a small angle between the aircraft track and the trough axis.

## Summary of Case Studies

Data for five other LTZ occurrences were gathered by similarly-instrumented aircraft in the same geographical area on February 19, 1968, February 20, 1968, February 26, 1970, January 20, 1971 and January 11, 1972. Cases fell into either the lee wave or hydraulic jump classifications suggested by Lilly and Vergeiner (1970). Differentiation of the two modes was difficult in a few analyses where it could not be ascertained whether the flow pattern was one of an undular jump or a large amplitude lee wave system. The major features of the clear cut cases have been combined in the schematic cross sections in Figure 10. Figures 10a–10c represent the wave type while Figure 10d represents the jump type. Characteristic values of various LTZ parameters are presented in Table 1.

The potential temperature field of Figure 9 shows the typically weak gradient within the LTZ and the relatively strong stability at the top. The potential temperature minima at low levels are interpreted as evidence of air moving upward from the surface layers in the rotor circulation. The streamlines in Figure 9 have been implied from the isentropic analyses and wind speed and direction variations. Single and multiple rotors were common in both the wave and jump cases. Roll clouds were present on several occasions, near the top of the LTZ, below the wave crests.

The wind speed maximum in the stable layer at the top of the LTZ (Figure 10b) was commonly associated with strong vertical shears and large longitudinal speed changes, especially in the vicinity of the updrafts and the rotor. Wind speed minima were well marked in the rotor and the 'toe roller' (or reversed rotor, Ball, 1956) in the first wave trough to the lee of the ridge.

In the wave cases, turbulence within

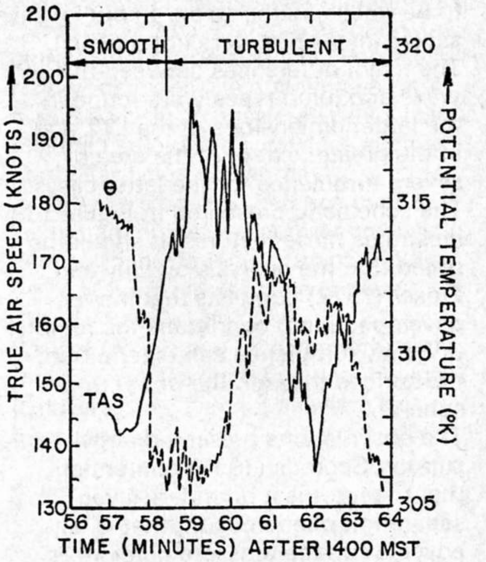

Figure 8. True Air Speed (solid line) and potential temperature (dashed line) records for upper flight track of cross section 3. The aircraft was flying downwind when these data were collected. One minute of flight time corresponds with a flight distance of about 6 km.

the LTZ reached moderate or greater intensities most frequently in the shaded regions of Figure 10c. The most common feature of the turbulence fields for all cases was the occurrence of severe turbulence in the updraft area just upstream of the rotor. On a few occasions, it was noticed that this maximum was separated by a less turbulent region from a second maximum in the vicinity of the potential temperature minimum at lower levels (see Figure 10a). Aside from the 'toe roller', some degree of patchy turbulence was found in the stable layer above the LTZ in all cases, probably due to strong shears induced by the lee waves. Turbulence patches tended

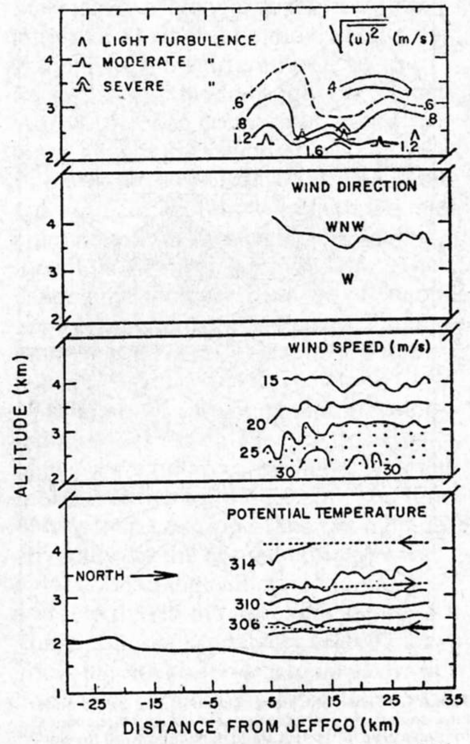

Figure 9. Cross section 4. Same as Figure 5, but for 1304–1336 MST.

to be smaller in the stable air but locally severe intensities were not unusual. The major differences between the wave and jump types were found in the larger dimensions of the LTZ and in the greater extent of the area of severe turbulence for the latter cases. The schematic presented in Figure 10d illustrates these features. It should be noted that the analysis by Lilly and Zipser (1972) suggests that in well-developed jump conditions the region of heavy turbulence can extend from the surface through the upper troposphere.

The observations presented above support Scorer's (1953) contention that the rotor is a boundary layer separation phenomenon; that is, an adverse surface pressure gradient is induced by the upper wave pattern and horizontal convergence in the lower levels leads to the injection of turbulent boundary layer air into the updraft region. It can be seen that any convection in the lowest layers will enhance the updraft turbulence.

In an effort to determine the role of the LTZ in the energetics of large scale atmospheric motion systems, dissipation estimates were made from 30 spectra of the longitudinal gust velocities measured within the LTZ. Utilizing inertial sub-range theory ranges of dissipation were estimated for light, moderate and severe turbulence (see Table). Assuming a mean depth of the LTZ of 3 km, dissipations of the order of 20–100 watts m$^2$ were found to be representative of the LTZ.

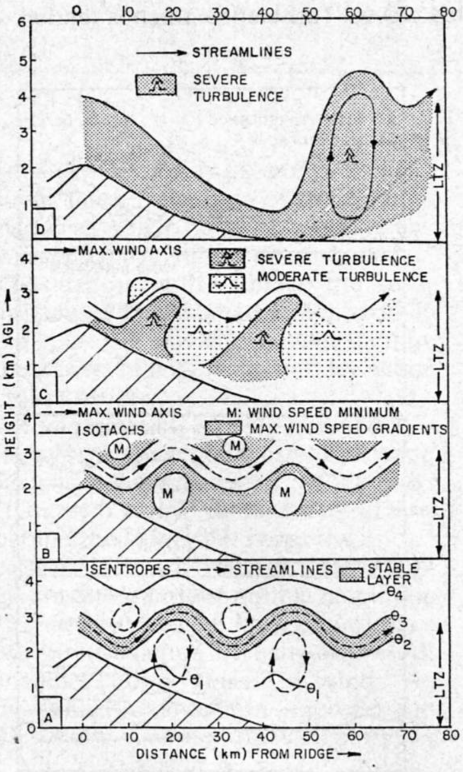

Figure 10. Schematic cross section of LTZ based on six case studies. A: potential temperature and streamlines for wave type. B: isotachs and maximum wind for wave type. C: turbulence distribution for wave type. D: streamlines and turbulence distribution for jump type.

**Table. Characteristics of the LTZ**

| Characteristic | | | | | | Remarks |
|---|---|---|---|---|---|---|
| Distance of first lee trough from ridge line: | 5 to ∾ 50 km | | | | | Largest in jump cases. |
| Length: | ∾ 25 to > 65 km | | | | | Measured downwind of first lee wave trough. Largest in jump cases. |
| Depth: | | | | | | |
| Below wave crest | < 1 to > 3 km AGL | | | | | Largest in jump cases. |
| Below wave trough | < 0.5 to 1 km AGL | | | | | |
| Typical mesoscale gradients at LTZ boundary: | | | | | | Based on low pass filtered data. |
| $\partial\Theta/\partial x$ | 5°K (10 km)$^{-1}$ | | | | | |
| $\partial\Theta/\partial z$ | 7°K (km)$^{-1}$ | | | | | |
| $\partial u/\partial x$ | $10^{-3}$ sec$^{-1}$ | | | | | |
| $\partial u/\partial z$ | $10^{-2}$ sec$^{-1}$ | | | | | |
| Turbulence: Frequency | % of flight distance | Height (km) AGL 0.4–1.4 | 1.4–2.4 | 2.4–3.4 | 0.4–3.4 | Based on three strong cases downstream of first lee wave trough. |
| | > Light | 99 | 99 | 92 | 96 | |
| | > Moderate | 66 | 46 | 35 | 48 | |
| | > Severe | 16 | 14 | 16 | 16 | |
| | Flight Distance (km) | 348 | 348 | 383 | 1079 | |
| Dissipation | | (cm$^2$/sec$^{-3}$) | | | | Based on 30 longitudinal gust spectra. |
| | Light | 7 to 66 | | | | |
| | Moderate | 121 to 310 | | | | |
| | Severe | 433 to 972 | | | | |

Since the LTZ is essentially a vertically exaggerated boundary layer, the above figures become significant when compared to the average boundary layer values estimated by Brunt (1952) and computed by Kung (1969) which are of the order of 1–5 watts m$^{-2}$. This would be especially true for long-lived, intense LTZ which tends to have large dimensions.

## Summary

The analysis of six cases of LTZ occurrences presented above has verified, quantitatively, many of the features of the LTZ known from previous studies (e.g.; Kuettner, 1939; Forchgott, 1949; Holmboe and Klieforth, 1957, Gerbier and Berenger, 1957). The fields of windspeed and turbulence within the LTZ have been analyzed in detail for the first time, allowing an estimate of mesoscale wind, temperature and turbulence gradients and giving a picture of the spatial distribution of the turbulence.

The observations were by no means complete. For example, rotor circulations could only be implied from the records of potential temperature and Doppler winds. Direct measurements of the rotor circulation via aircraft instrumented with inertial platforms or by means of radar tracking of chaff or balloons should contribute to the understanding of the LTZ.

An estimate of the kinetic energy dissipation within the LTZ suggests that that phenomenon may play an important role in the large scale atmospheric kinetic energy budget, especially in strong cases. It is recommended that an effort be made to determine the frequency of occurrence, the dimensions and overall strength of the LTZ as a function of synoptic conditions and geographical area, in order to obtain a better estimate of its importance in the atmospheric energy budget and to allow the realistic parameterization of its effects on larger scales.

## Acknowledgements

The authors are indebted to Drs. D. K. Lilly, E. Zipser and P. Julian of NCAR for providing the aircraft data. The Northern Regional Data Center of the California State Universities and Colleges and National Center for Atmospheric Research are acknowledged for the use of their computer facilities. D. Ballanti aided in the computations and the preparation of analyses. Dr. A. Miller and Dr. D. K. Lilly made many useful suggestions during the course of the study. Drafting was done by Mrs. O. F. Koonce and the manuscript was typed by Mrs. L. F. LaDuca. The study was sponsored by the National Science Foundation under Grant GA-32403.

### References

Alaka, M. A., 1960: The airflow over mountains. *Tech. Note No. 34,* World Meteorological Organization, Geneva, Switzerland, 135 pp.

Ball, F. K., 1956: The theory of strong katabatic winds. *Austral. J. Phys., 9,* 373–385.

Brunt, D., 1941: *Physical and Dynamical Meteorology.* Cambridge University Press, 428 pp.

Burris, R. H., J. C. Covington, M. N. Zrubek, 1973: Beechcraft Queen Air Aircraft. *Atmospheric Technology,1,* 25-27.

Fingerhut, W. A., and P. F. Lester, 1973: Lower turbulent zones associated with mountain lee waves. *Paper No. 30,* Department of Meteorology, California State University, San Jose. Research conducted under NSF Grant GA-32403, 118 pp.

Forchtgott, J., 1949: Wave streaming in the lee of mountain ridges. *Bull. Meteor. Czech.* Prague, *3,* p. 49.

Gerbier, N., and M. Berenger, 1957: Les ondes dues au relief dans les Basses-Alpes françaises. 2$^e$ campagne d'études et de mesures, janvier–fevrier 1957. Direction de la Météorologie Nationale.

Holmboe, L. and H. Klieforth, 1957: Investigation of mountain lee waves and the airflow over the Sierra Nevada. *Final Report,* Contract AF19(604)–728, Department of Meteorology, University of California, Los Angeles, 290 pp.

Kuettner, J., 1939: Zur Entstehung der Föhnwelle. *Beit. Phys. Atmos., 25,* 251–299.

Kuettner, J., 1959: The rotor flow in the lee of mountains. *G. R. D. Research Notes No. 6,* Air Force Cambridge Research Center, Cambridge, 20 pp.

Kuettner, J., and D. K. Lilly, 1968: Lee waves in the Colorado Rockies. *Weatherwise, 21,* 180–195.

Kung, E. C., 1969: Further studies of the kinetic energy balance. *Mon. Wea. Rev., 97,* 573–581.

Lester, P. F., 1972: An energy budget for intermittent turbulence in the free atmosphere. *J. Appl. Meteor., 11,* 90–98.

Lilly, D., Y. Pann, P. Kennedy, and W. Toutenhoofd, 1971: Data Catalog for the 1970 Colorado Lee Wave Observational Program. *NCAR-TN/STR-72.* 190 pp.

Lilly, D. K., and E. J. Zipser, 1972: The Front Range Windstorm of 11 January 1972 – A meteorological narrative. *Weatherwise, 25,* 56–63.

Scorer, R. S., 1955: The theory of airflow over mountains – IV. Separation of flow from the surface. *Quart. J. Roy. Meteor. Soc., 81,* 340–350.

Vergeiner, I., and D. K. Lilly, 1970: The dynamic structure of lee wave flow as obtained from balloon and airplane observations. *Mon. Wea. Rev., 98,* 44–58.

Vinnechenko, N. K., N. Z. Pinus, S. M. Schmeter, and G. Shur, 1973: *Turbulence in the Free Atmosphere.* English translation, J. Dutton, Ed. Plenum Press, N.Y., 260 pp.